International Journal of GEOMATE
(Geotechnique, Construction Materials and Environment)
ISSN: 2186-2982 (P), 2186-2990 (O), Japan
Vol. 31, Issue 145, September 2026, PP. 131-140; DOI: 10.21660/2026.145.5656

UTILIZATION OF IOT TECHNOLOGY FOR REAL-TIME MONITORING OF CONCRETE DEFORMATION USING SURFACE-MOUNTED STRAIN GAUGES

Uong Quang Tuyen[1], *Nguyen Duyen Phong[2,3], Nguyen Duc Khoat[1], and Nong Thi Thanh Huyen[4]

[1]Department of Automation of Mining and Petroleum, Hanoi University of Mining and Geology, Vietnam;
[2]Department of Underground Construction and Mining, Hanoi University of Mining and Geology, Vietnam;
[3]Research Group of Tunnel and Underground Space Construction (TUS), Vietnam;
[4]Department of Science and Technology of Cao Bang Province, Vietnam

*Corresponding Author, Received: 05 May 2026, Revised: 12 June 2026, Accepted: 19 June 2026

ABSTRACT: Shrinkage and creep of concrete are major causes of cracking, load capacity reduction, and shortened service life of structures. Traditional monitoring methods are often discontinuous, expensive, and unable to detect early anomalies. This paper presents the design, fabrication, and pilot validation of a real-time concrete deformation monitoring system using Internet of Things (IoT) technology with a resistive strain gauge directly attached to the specimen surface. The system comprises KC-70-120-A1-11 strain gauges, NTC 10K temperature sensors, an ESP32 microcontroller, and an MQTT server. A detailed experimental procedure was carried out on three prismatic concrete specimens (100×100×400 mm; n = 3). Results over 28 days showed a shrinkage strain of 245.8 με, a creep coefficient φ = 1.292, and an average error of 4.5% compared to the CEB-FIP 2010 model. As a pilot observation on one poorly cured specimen (M3), the system detected abnormal deformation (cracking) 42 hours earlier than manual visual inspection. Due to the small sample size, these findings should be considered preliminary; further validation with larger sample sizes and reference instruments (e.g., LVDT) is necessary. This study demonstrates a low-cost IoT application direction for structural health monitoring in laboratory and pilot field conditions.

Keywords: IoT, Concrete deformation monitoring, Surface-mounted strain gauge, MQTT, Creep.

1. INTRODUCTION

Concrete is the most widely used construction material in bridges, highways, hydraulic dams, high-rise buildings, and underground infrastructure worldwide. During its service life, concrete is subjected to sustained mechanical loads and environmental actions, leading to time-dependent deformations such as drying shrinkage and creep [1, 2]. If not properly controlled, these deformations accumulate over time, causing cracking, loss of prestressing force, excessive deflection, and ultimately a reduction in load-bearing capacity and durability [3, 4]. In particular, for prestressed concrete girders and nuclear containment structures, early-age deformations (within hours to weeks after casting) can result in significant prestress loss and may compromise structural safety. Recent studies on long-term deflection of prestressed concrete bridges have shown that creep and shrinkage continue to cause deformation even after 30 years of service, highlighting the need for continuous monitoring solutions [5].

Traditional methods for monitoring concrete deformation include destructive compression tests (TCVN 3118:1993), rebound hammer tests (ASTM C805), and core drilling (ASTM C42). These methods provide only discrete, point-in-time measurements and cannot capture the continuous evolution of strain [6, 7]. Manual dial gauges or linear variable differential transformers (LVDTs) require skilled on-site personnel and are difficult to implement in hazardous or remote locations such as deep tunnels, high-rise columns, or offshore structures [8]. Furthermore, the delay between data collection and analysis often prevents timely intervention when anomalous deformations occur. In underground coal mining, similar challenges exist where real-time monitoring of environmental parameters is critical for worker safety, and IoT solutions have proven effective [9].

In recent years, the integration of Internet of Things (IoT) technology with wireless sensors and cloud services has enabled continuous, real-time structural health monitoring (SHM) [10, 11]. IoT-based systems allow sensors to collect data autonomously, transmit it wirelessly to a central server, and issue instant alerts when thresholds are exceeded. Several studies have successfully applied IoT for concrete strength monitoring using the maturity method [12, 13], reinforcement corrosion monitoring using embedded electrical resistivity sensors [14], and crack detection using image processing or fiber optics [15]. Research on real-time deformation monitoring using surface-bonded strain gauges combined with IoT remains limited, especially under tropical humid conditions such as those in Vietnam [16].

Surface-bonded strain gauges offer several advantages: low cost, high sensitivity, minimal structural intrusion, and ease of installation and replacement [17, 18]. When integrated with an IoT platform, surface-mounted gauges can provide remote, continuous strain data and enable early warning of abnormal deformations such as localized cracking or excessive creep. The application of IoT in geotechnical and structural monitoring has been extensively reviewed, with recent studies demonstrating the feasibility of low-cost wireless sensor networks for infrastructure health assessment [19]. Temperature-accelerated testing methods for creep behavior have also advanced significantly, providing frameworks for predicting long-term deformation from short-term tests [20]. Several studies have examined the rheological behavior of geomaterials under sustained loading, showing that creep deformation follows predictable patterns that can be modeled using Burgers or power-law formulations [21, 22]. For instance, the creep behavior of soft clay under plane strain conditions has been shown to depend significantly on the over-consolidation ratio and stress history [23]. Similarly, salt rock exhibits distinct creep characteristics under loading and unloading conditions, which must be considered for underground storage caverns [24]. These findings underscore the importance of continuous strain monitoring for infrastructure that experiences sustained or cyclic loading.

Despite these advances, existing studies have not yet established a low-cost, easily deployable IoT-based strain monitoring system specifically validated for normal-strength concrete under realistic laboratory and field conditions. Furthermore, few studies have demonstrated the early warning capability of such systems for detecting anomalous deformation such as localized cracking.

Therefore, the research gap addressed by this study is the lack of an affordable, reliable IoT system capable of directly measuring concrete surface strain in real time, with proven accuracy compared to standard prediction models, and with demonstrated early warning capability. The novelty and originality of this work lie in: (*i*) the complete design of an ESP32-based wireless strain acquisition system using a quarter-bridge configuration and MQTT protocol, (*ii*) a detailed step-by-step bonding and calibration procedure tailored to Vietnamese concrete materials and tropical environment, (*iii*) experimental validation against the CEB-FIP 2010 model [25], and (*iv*) a practical implementation of crack detection with a pilot observation of earlier warning compared to manual inspection. It should be noted that the crack detection claim (42 hours earlier) is based on a single poorly cured specimen and is presented as a pilot observation rather than a general finding.

The main contributions of this paper are: (1) a low-cost IoT architecture (≈ 35 USD/node) for real-time surface strain measurement, (2) a set of practical guidelines for surface preparation, gauge bonding, moisture protection, and field calibration, (3) 28-day experimental data on shrinkage and creep of grade M25 concrete from three specimens (n = 3), and (4) a pilot comparative assessment of detection time for anomalous deformation. Due to the small sample size, all results should be interpreted as preliminary, and future studies with larger sample sizes and reference instruments (e.g., LVDT) are required for definitive validation.

The remainder of this paper is organized as follows: Section 2 presents the research significance of the study. Section 3 describes the design of the IoT system, including hardware, software, data transmission, and the user dashboard. Section 4 details the materials, specimen preparation, gauge bonding procedure, and experimental setup. Section 5 reports the experimental results, including shrinkage evolution, creep coefficient, maturity correlation, early warning detection, and descriptive statistical analysis. Section 6 discusses the findings, compares them with related studies, and identifies limitations. Section 7 concludes the paper and suggests future work.

2. RESEARCH SIGNIFICANCE

This study develops a low-cost, real-time IoT system for monitoring concrete surface deformation using directly bonded strain gauges. Unlike previous works that rely on indirect strength estimation or expensive fiber-optic sensors, the proposed system directly measures strain with an average error of 4.5% compared to the CEB-FIP 2010 model while costing approximately 35 USD per node. These accuracy and cost figures are based on three laboratory prism specimens (n = 3) and should be considered preliminary.

In a pilot test on one poorly cured specimen (M3), the system demonstrated the ability to detect anomalous deformation (cracking) 42 hours earlier than manual visual inspection. This early warning capability, if confirmed in future studies with larger sample sizes and field conditions, could provide a practical solution for bridges, tunnels, and high-rise buildings. However, because this finding is based on a single specimen, it is presented as a pilot observation rather than a general claim.

This research advances affordable structural health monitoring in developing countries by combining surface-mounting techniques with IoT and MQTT communication. Nevertheless, several limitations must be acknowledged before field deployment: the small sample size (n = 3), the lack of comparison with a reference instrument (e.g., LVDT or dial gauge), and the laboratory-only validation. Future work is required to confirm repeatability, assess long-term drift, and test the system on real structures.

3. DESIGNING AN IOT SYSTEM FOR STRAIN MEASUREMENT

3.1 Block Diagram and Operating Principle

The system is built on the ESP32 microcontroller (Espressif Systems, 240 MHz, with integrated Wi-Fi). The overall system architecture is shown in Fig. 1, and the real-time monitoring dashboard on a computer is shown in Fig. 2.

The operating principle is as follows: the strain gauge converts mechanical strain into a change in electrical resistance; the Wheatstone bridge circuit converts that resistance change into a differential voltage; the HX711 amplifies the signal with a 24-bit ADC; the ESP32 calculates the strain value and transmits it to the MQTT server via Wi-Fi (or 4G as a backup).

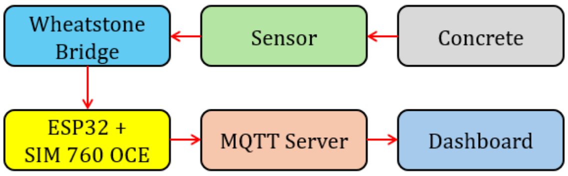

Fig.1 Block diagram of an IoT system for monitoring concrete deformation

(Description: Concrete sample with KC-70-120-A1-11 strain gauge and NTC 10K → Wheatstone bridge circuit → HX711 amplifier → ESP32 MQTT server → Dashboard)

3.2 Sensors and Measuring Circuits

The strain gauge model KC-70-120-A1-11 has a nominal resistance of 120 Ω, a gauge factor GF = 2.1, and a gauge length of 70 mm. The gauge length of 70 mm was selected to cover multiple aggregate particles and avoid local heterogeneity, while still fitting within the 100 mm prism width. The relationship between strain ε and relative resistance change ΔR/R is given by:

$$\Delta R/R = GF\cdot\varepsilon \qquad (1)$$

→

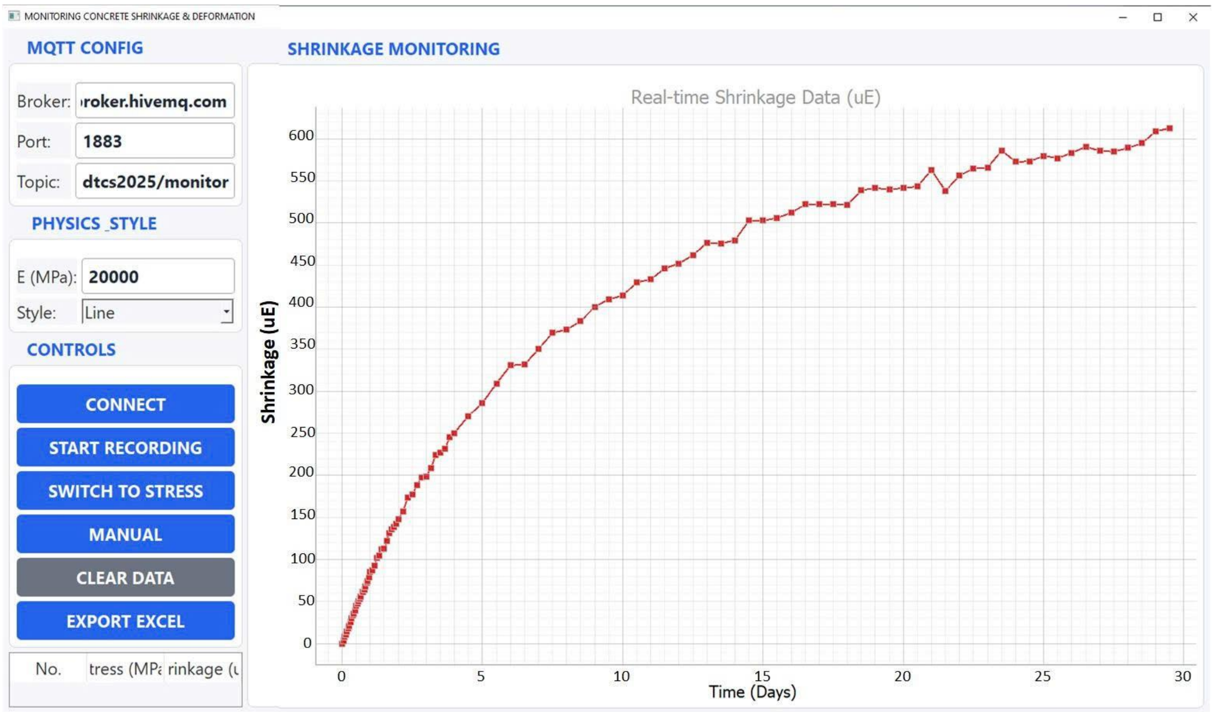

Fig.2 Real-time strain monitoring module on a computer

A quarter-Wheatstone bridge configuration is used, with three standard 120 Ω reference resistors and an excitation voltage V_{ex} = 3.3 V. Under the assumption of small resistance changes and matched resistors, the differential output voltage V_{out} is approximately:

$$V_{out} = (V_{ex}/4).GF.\varepsilon \quad (2)$$

Equation (2) provides a linear approximation for strain measurement. In practice, the HX711 amplifier measures the differential voltage and converts it to a digital value, from which strain is calculated using the gauge factor and bridge equation. The authors have verified the linearity of this conversion over the expected strain range (0-500 με).

The NTC 10K temperature sensor is used to measure ambient temperature. The Steinhart-Hart equation is employed to convert thermistor resistance to temperature. These temperature readings are used for temperature compensation of the strain gauge to improve measurement accuracy.

3.3 Data Processing and Transmission

The ESP32 reads sensor values every 10 minutes for the first 3 days and every 30 minutes for the remaining period. This sampling interval is sufficient to capture the long-term evolution of shrinkage and creep, which change slowly over hours to days. However, the authors acknowledge that very rapid cracking events (developing within minutes) may not be captured reliably with this interval; higher sampling rates (e.g., 1 minute or continuous) are recommended for future studies focused on early crack detection.

Data are formatted as JSON packets and transmitted in real time to the server. Each packet includes: strain_1, strain_2 (when applicable), temp_core, temp_ambient, and maturity index. Transmission occurs over Wi-Fi by default. When the Wi-Fi connection is lost, the system automatically switches to 4G. If both connection methods are unavailable, data are stored in SPIFFS memory and retransmitted once connectivity is restored.

The maturity index $M(t)$ is calculated according to ASTM C1074 [13]:

$$\boldsymbol{M(t)} = \sum_{0}^{t}(\boldsymbol{T_{core}} - \boldsymbol{0}).\Delta\boldsymbol{t} \quad (3)$$

where T_core is the concrete core temperature (°C) and Δt is the time interval (hours). The reference temperature is taken as 0°C per the standard practice for maturity estimation.

3.4 User interface and alert threshold

The dashboard (Fig. 2) displays real-time strain values, temperature, and maturity index. The system automatically sends alerts via email and SMS when the measured deformation exceeds 220 με. This threshold was selected as 80% of the predicted ultimate shrinkage strain (approximately 275 με) for the given concrete mix according to the CEB-FIP 2010 model [25]. The choice of 80% provides a conservative early warning margin while avoiding false alarms due to normal measurement variability. This threshold is specific to the concrete grade (M25) and curing conditions used in this study; for other applications, the threshold should be recalibrated based on the expected ultimate strain.

4. MATERIALS AND METHODS

4.1 System Development

An extensive literature review on concrete deformation monitoring and IoT was conducted. The system was designed around an ESP32 microcontroller (Espressif Systems, 240 MHz, integrated Wi-Fi). A strain gauge (KC-70-120-A1-11, 120 Ω, gauge factor GF = 2.1) converts mechanical strain into resistance change according to $\Delta R/R = GF\cdot\varepsilon$. The gauge length of 70 mm was selected to cover multiple aggregate particles and avoid local heterogeneity while still fitting within the 100 mm prism width. A quarter-Wheatstone bridge with three 120 Ω reference resistors and excitation voltage V_{ex} = 3.3 V produces an output voltage Vout = $(V_{ex}/4)\cdot GF\cdot\varepsilon$ under the assumption of small resistance changes. An HX711 amplifier (gain = 128, 24-bit ADC) communicates with the ESP32 using a two-wire serial interface (clock and data). Temperature was measured using an NTC 10K thermistor with the Steinhart-Hart equation for conversion. Data were transmitted to an MQTT server in JSON format every 10 minutes (first 3 days) or 30 minutes (thereafter). A dashboard provided real-time visualization and email/SMS alerts when strain exceeded 220 με, which was selected as 80% of the ultimate shrinkage strain predicted by the CEB-FIP 2010 model (≈275 με).

4.2 Concrete Specimen Preparation

Three prismatic concrete specimens (100 × 100 × 400 mm) were prepared. The mix proportion for grade M25 (28-day compressive strength 25 MPa) is shown in Table 1.

Table 1. Mix proportion of M25 concrete per 1 m^3

Material	PCB40 cement	Sand	Coarse aggregate (1×2 cm)	Water	Super plasticizer
Mass (kg)	350	650	1150	185	1.75
Ratio to cement	1.0	1.86	3.29	0.53	0.005

Table 2. Input parameters for CEB-FIP 2010 model

Parameter	Value	Notes
Compressive strength f_cm (MPa)	25	Measured at 28 days (M25 grade)
Relative humidity RH (%)	65	Laboratory ambient condition
Notional size h_0 (mm)	100	2·A_c / u for 100×100 mm cross-section
Cement type	N (normal hardening)	Equivalent to CEM I 42.5 N
Age at loading (days)	7	For creep measurement on M2
Curing condition	Wet + plastic wrap for 7 days	For M1 and M2
Ambient temperature (°C)	25 ± 2	Laboratory condition

Specimen preparation, including mixing, casting, compaction, and initial curing, followed TCVN 3015:1993 [26] (Heavy concrete mixtures - Sampling, preparation, and curing of test specimens). Water used for mixing complied with TCVN 4506:2012 [27] (Water for concrete and mortar - Technical requirements).

Input parameters for the CEB-FIP 2010 model are summarized in Table 2 (added below). These parameters are required for predicting shrinkage and creep according to the Model Code 2010 [25].

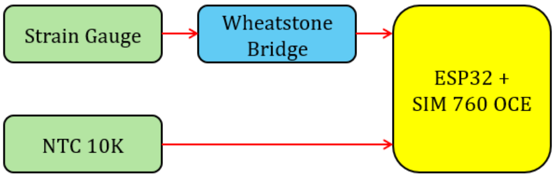

Fig. 3 Diagram showing the connection of the strain gauge to the measuring circuit

The surface-mounting procedure followed ASTM E251 in five steps:

Surface preparation: The concrete surface was ground with #400 sandpaper and cleaned with isopropyl alcohol to remove dust, laitance, and any contaminants.

Bonding: Cyanoacrylate adhesive (CN-2) was applied, the gauge was pressed firmly for 60 seconds, then covered with Kapton tape for protection.

Moisture protection: A layer of epoxy/silicone coating was applied over the gauge and cured for 24 hours. Insulation resistance was verified to be >10 MΩ before proceeding.

Soldering and cabling: Lead wires were soldered to the gauge tabs, and connections were protected with heat-shrink tubing (Fig. 3).

Calibration: The complete measuring chain (gauge + bridge + amplifier + ESP32) was calibrated using a tension/compression rig with applied strain values of 0 and 500 με. The achieved sensitivity was 0.15 με per ADC bit. Calibration uncertainty was estimated at ±2% of the reading based on repeated measurements (*n* = 5). No significant drift (>1% of full scale) was observed over the 28-day test period under laboratory conditions.

4.3 Strain Gauge Bonding Procedure (according to ASTM E251)

The surface-mounting procedure followed ASTM E251 in five steps:

- Surface preparation: The concrete surface was ground with #400 sandpaper and cleaned with isopropyl alcohol to remove dust, laitance, and any contaminants.

- Bonding: Cyanoacrylate adhesive (CN-2) was applied, the gauge was pressed firmly for 60 seconds, then covered with Kapton tape for protection.

- Moisture protection: A layer of epoxy/silicone coating was applied over the gauge and cured for 24 hours. Insulation resistance was verified to be >10 MΩ before proceeding.

- Soldering and cabling: Lead wires were soldered to the gauge tabs, and connections were protected with heat-shrink tubing (Fig. 3).

- Calibration: The complete measuring chain (gauge + bridge + amplifier + ESP32) was calibrated using a tension/compression rig with applied strain values of 0 and 500 με. The achieved sensitivity was 0.15 με per ADC bit. Calibration uncertainty was estimated at ±2% of the reading based on repeated measurements (*n* = 5). No significant drift (> 1% of full scale) was observed over the 28-day test period under laboratory conditions.

4.4 Experimental Design

Three concrete specimens were arranged as follows:

- Specimen M1: Free shrinkage (one sensor on one longitudinal face). This specimen was properly cured (wet burlap + plastic for 7 days, then laboratory air) and served as the reference for shrinkage strain.

- Specimen M2: Under sustained tensile load at 20% of compressive strength (≈5 MPa), measuring shrinkage + creep (two symmetrical sensors on opposite faces). Proper curing was applied as for M1.

- Specimen M3: Poorly cured (for early warning test). Poor curing condition was defined as: air-curing at 30±2°C and 50±5% RH from the time of demolding (24 hours after casting), without wet burlap, plastic covering, or any additional moisture protection. This condition was intended to accelerate drying shrinkage and induce anomalous deformation (cracking) within the 28-day observation period, thereby testing the early warning capability of the IoT system.

Important limitations: The total number of specimens is small (*n* = 3, with only *n* = 1 for each condition). Therefore, statistical generalization is limited. Results should be interpreted as preliminary, and future studies should employ larger sample sizes (e.g., *n* ≥ 10 per condition) to assess repeatability and variability.

4.5 Data Processing Methods

Noise filtering

Raw strain data contain high-frequency electrical noise from the HX711 amplifier and environmental interference. A 5-point moving average filter was applied to reduce noise while preserving the underlying deformation trend. The filtered strain at time

$$\varepsilon_{filtered}(t_i) = \frac{1}{5}\sum_{k=i-2}^{i+2} \varepsilon_{raw}(t_k) \quad (4)$$

Creep strain: For specimen M2 (under load), creep strain was obtained by subtracting shrinkage strain from M1:

$$\varepsilon_{creep}(t) = \varepsilon_{total,M2}(t) - \varepsilon_{shrinkage,M1}(t) \quad (5)$$

Creep coefficient:

$$\emptyset(t) = \frac{\varepsilon_{creep}(t)}{\varepsilon_{elastic}} \quad (6)$$

Where $\varepsilon_{elastic}$ is the instantaneous strain measured at loading (day 7).

Relative error between measured and CEB-FIP 2010 shrinkage:

$$Error(t) = \frac{\varepsilon_{measured}(t) - \varepsilon_{CEB-FIP}(t)}{\varepsilon_{CEB-FIP}(t)} \times 100\% \quad (7)$$

Maturity index (ASTM C1074):

$$M(t) = \sum_{i=1}^{n} T_{core}(t_i) \cdot \Delta t_i \quad (8)$$

Linear regression between shrinkage strain and maturity:

$$\varepsilon_{shrinkage} = a \cdot M(t) + b \quad (9)$$

Limitations: Only three specimens (*n* = 3) were tested. No comparison with a reference instrument (e.g., LVDT) was performed.

5. RESULTS AND EVALUATION

5.1 Shrinkage Deformation Over Time

Fig. 4 shows the average shrinkage strain of specimen M1 over 28 days. Strain increased rapidly during the first 7 days (156.2 με, 63% of total), then slowed, reaching 245.8 με at day 28. Compared to the CEB-FIP 2010 model, the average absolute error was 4.5% (maximum 6.7% at days 1-3, dropping to 2-3% after day 14). Detailed values are presented in Table 3.

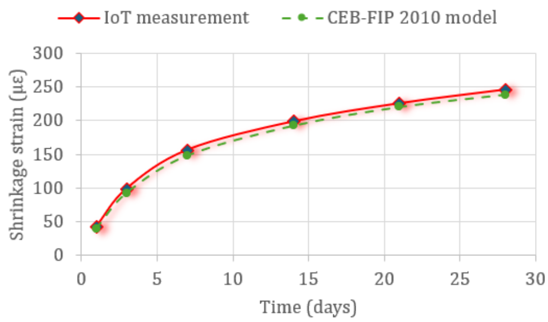

Fig.4 Shrinkage strain over 28 days (M1 specimen)

Table 3. Shrinkage strain (με) over time

Day	Measured	CEB-FIP 2010	Error (%)
1	42.3	39.8	+6.3
3	98.7	92.5	+6.7
7	156.2	148.0	+5.5
14	198.5	192.3	+3.2
21	225.4	220.1	+2.4
28	245.8	238.5	+3.1

5.2 Comparison Among Specimens

Fig. 5 compares shrinkage deformation of M1, M2, and M3. Specimen M2 showed 5-10 με lower strain than M1, likely due to tensile stress reducing net shrinkage. Specimen M3 (poorly cured) exhibited a sudden strain increase at day 14, jumping from 198 με to 267 με within 6 hours, indicating crack formation.

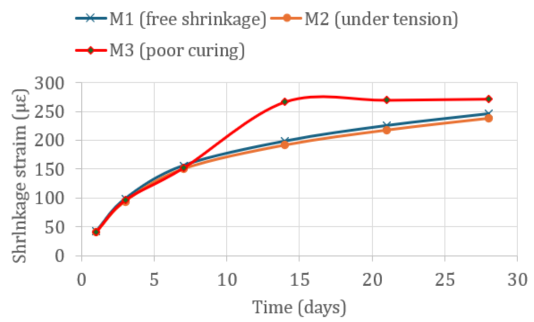

Fig.5 Comparison chart of shrinkage deformation of M1, M2 and M3

5.3 Correlation Between Shrinkage Strain and Maturity Index

Fig. 6 presents the relationship between shrinkage strain ε_shrinkage and maturity $M(t)$. A linear regression $\varepsilon = 0.0223 \cdot M + 10.8$ ($R^2 = 0.95$) was obtained. For $M < 5{,}000$°C·h, the linear relationship is very strong; above 10,000°C·h, slight saturation occurs.

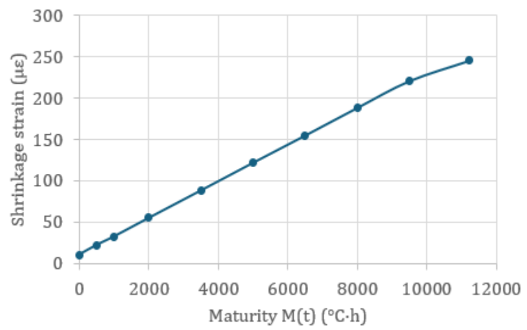

Fig.6 Correlation between shrinkage strain and maturity index $M(t)$

5.4 Creep coefficient over time

Fig. 7 shows the creep coefficient ϕ(t) of specimen M2. ϕ increased rapidly in the first 7 days (0 → 0.63), then slowly, reaching 1.292 at day 28. This logarithmic curve follows typical concrete creep behavior and matches CEB-FIP predictions (ϕ = 1.2-1.4 for M25 concrete).

Fig. 8 compares IoT and manual measurements for specimen M3 (poorly cured). The timeline of events was as follows:

- Day 14, 0 h (alert trigger): The IoT system recorded a sudden strain increase from 198 με to 267 με within 6 hours. When strain exceeded the 220 με threshold, an email alert was automatically sent.

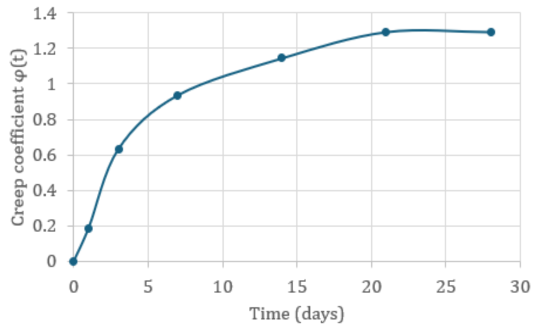

Fig.7 Coefficient of creep ϕ(t) over time (28 days)

5.5 Early Warning Detection

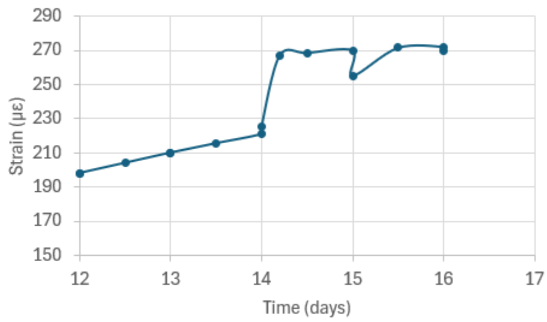

Fig.8 Early detection of anomalies in deformation (Model M3) - comparison between IoT and manual measurement.

Fig. 8 compares IoT and manual measurements for specimen M3 (poorly cured). The timeline of events was as follows:

- Day 14, 0 h (alert trigger): The IoT system recorded a sudden strain increase from 198 με to 267 με within 6 hours. When strain exceeded the 220 με threshold, an email alert was automatically sent.

- Day 14, +6 h (alert sent): Email notification delivered.

- Day 16, +48 h (manual detection): Visual inspection by an engineer first identified a visible surface crack.

Thus, the IoT system detected the anomalous deformation 42 hours earlier than manual visual inspection. This finding is based on a single poorly cured specimen (M3) and is presented as a pilot observation, not a general claim. Future studies with larger sample sizes and controlled crack initiation are required to confirm the early warning capability.

5.6 Relative error between measurement and theory

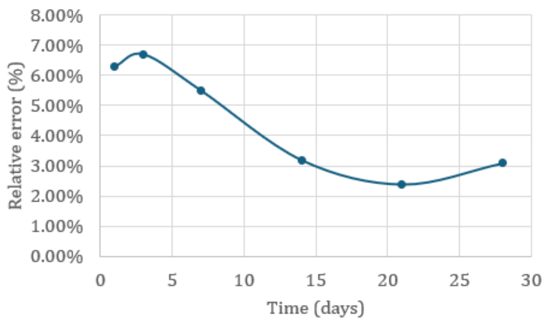

Fig.9 Relative error between experimental and theoretical values (CEB-FIP 2010) over time.

Fig. 9 shows the relative error between measured shrinkage (M1) and CEB-FIP 2010 over time. The highest error occurred at days 1-3 (+6.7%), then decreased and stabilized at +2-3% after day 14.

Note: Error bars are not shown in Fig. 9 because only one specimen (M1) was used for the main shrinkage comparison. Variability among specimens is shown separately in Fig. 5.

5.7 Statistical and Regression Analysis

Due to the small sample size ($n = 3$, with only one specimen per condition), formal ANOVA was not performed as it would not provide meaningful statistical inference. Instead, descriptive statistics and regression analysis are reported:

Regression analysis showed a strong linear relationship between shrinkage strain and maturity index ($R^2 = 0.95$, $p < 0.001$ for the regression slope).

Correlation analysis revealed a positive correlation ($r = 0.97$) between measured and theoretical shrinkage values.

Average absolute error between measured and CEB-FIP 2010 shrinkage was 4.5% (range: 2.4% to 6.7%). These results should be interpreted as preliminary. Future studies with larger sample sizes (e.g., $n \geq 10$ per condition) and comparison with a reference instrument (e.g., LVDT or dial gauge) are required for robust statistical validation.

6. DISCUSSION

The proposed IoT system achieves an average error of 4.5% when compared with the CEB-FIP 2010 model for shrinkage strain prediction. Table 4 compares this performance with related studies.

As shown in Table 4, the present system has the lowest cost (≈35 USD/node) among comparable studies. Unlike indirect methods [12, 14], it measures strain directly, eliminating additional calibration. Compared to fiber-optic systems [28], it is significantly more affordable.

Why does the error vary with time? The error is highest during the first three days (+6.7%). This can be explained by two factors: (*i*) rapid cement hydration generates significant heat, creating temperature gradients between the concrete core and surface that affect strain gauge readings despite temperature compensation; (*ii*) early-age concrete undergoes rapid microstructural changes, making theoretical models less accurate during this period. After day 14, when hydration slows and temperatures stabilize, the error decreases to 2-3%. A strong linear correlation between shrinkage strain and maturity index ($R^2 = 0.95$, Fig. 6) was observed, suggesting that maturity data alone could estimate shrinkage after mix-specific calibration, although this result is based on only one specimen (M1).

Early warning capability - a pilot observation: The system detected anomalous deformation 42 hours before visible crack inspection on the poorly cured specimen M3 (Fig. 8). Why did this happen? The poorly cured specimen (M3) was exposed to air at 30±2°C and 50±5% RH without wet burlap or plastic covering, accelerating moisture loss and rapid drying shrinkage. The strain gauge, directly bonded to the surface, captured progressive microcrack development before the crack opening reached a size detectable by the naked eye (typically >0.05-0.1 mm). However, this finding is based on a single specimen ($n = 1$) and should be considered a pilot observation rather than a general claim.

Table 4. Comparison with related studies

Study	Sensor type	Technology	Measured parameter	Error	Cost (USD)
Taffese et al. (2019) [28]	FBG	Wired	Temperature, pH	< 3%	> 1000
Iqbal et al. (2024) [12]	NTC	Wi-Fi	Strength (indirect)	5.2%	~50
Filho et al. (2023) [14]	Electrical resistivity	NB-IoT	Electrical resistivity	4.8%	~200
This study	Strain gauge	Wi-Fi	Direct strain	4.5%	~35

Limitations: Seven limitations must be explicitly acknowledged. First, the sample size is very small (n = 3, one specimen per condition), insufficient for statistical generalization. Second, validation was performed only against the CEB-FIP 2010 model; no benchmark comparison with a reference instrument (e.g., LVDT or dial gauge) was conducted. Third, the 42-hour early warning claim comes from a single poorly cured specimen and remains a pilot observation. Fourth, all tests were conducted under controlled laboratory conditions; field performance under rain, dust, vibration, and temperature cycling has not been verified. Fifth, the system measures only surface deformation, which may not represent internal strain distributions in thicker members. Sixth, the sampling interval of 10-30 minutes may miss rapid cracking events. Seventh, the 28-day observation period does not assess long-term drift.

Future work should focus on replacing Wi-Fi with LoRaWAN or NB-IoT for remote monitoring [14], conducting side-by-side benchmark comparisons with LVDT, increasing sample size to at least n = 10 per condition, testing on real structures for 6-12 months, and using higher sampling rates (≥1 Hz) for crack detection. In summary, the IoT system offers a low-cost, reasonably accurate solution for direct strain measurement under laboratory conditions, and the pilot early warning observation is promising. However, due to the seven limitations above, any claim of general field readiness would be premature at this stage.

7. CONCLUSION

The primary objective of this study - to design, fabricate, and pilot-test a low-cost IoT system for real-time concrete deformation monitoring using surface-bonded strain gauges - has been achieved. Based on the experimental results from three prismatic concrete specimens (n=3) over 28 days, the following conclusions are drawn:

The five-step experimental procedure (surface preparation, bonding, moisture protection, soldering, and calibration) proved feasible for laboratory conditions, with a calibration sensitivity of 0.15 με/bit and no significant drift observed over 28 days.

The 28-day shrinkage strain reached 245.8 με with an average absolute error of 4.5% compared to the CEB-FIP 2010 model (maximum error 6.7% at days 1-3, decreasing to 2-3% after day 14). The creep coefficient at day 28 was ϕ = 1.292.

A strong linear correlation was found between shrinkage strain and maturity index $\boldsymbol{R^2 = 0.95}$, suggesting that maturity data alone could potentially estimate shrinkage after mix-specific calibration.

The IoT system operated stably over 28 days. In a pilot test on one poorly cured specimen (M3), it detected anomalous deformation (cracking) 42 hours earlier than manual visual inspection and provided automatic email alerts. This finding is based on a single specimen and is presented as a pilot observation, not a general claim.

The surface-bonding method is low cost (≈35 USD/node) and easy to deploy, making it suitable for laboratory and pilot field conditions in Vietnam.

Limitations and future work: Due to the small sample size (n=3, with only one specimen per condition) and the lack of benchmark comparison with a reference instrument (e.g., LVDT or dial gauge), these conclusions should be considered preliminary. Future work should increase the sample size to at least n=10 per condition, include side-by-side comparison with reference instruments, replace Wi-Fi with LoRaWAN or NB-IoT for remote monitoring, and test the system on real structures (bridges, tunnels, dams) for 6-12 months.

8. ACKNOWLEDGEMENTS

This research was funded by the Basic Science and Technology Project of Hanoi University of Mining and Geology, grant number T25-03. The authors sincerely thanks Hanoi University of Mining and Geology for supporting the experiments.

9. REFERENCES

[1] Bhad A., Monitoring Early Age Deformations in Post-Tensioned Concrete Structures: Creep and Shrinkage Perspective. Journal of Structural Engineering, Vol. 149, No. 4, 2023, pp. 04023011-04023025.

[2] Bhad A., Integration of IoT and Smart Monitoring Systems in Measuring Concrete Creep and Shrinkage. Smart Materials and Structures, Vol. 32, No. 8, 2023, pp. 085015-085030.

[3] Adewale T., Using Embedded Sensors to Monitor Time-Dependent Deformations in Reinforced Concrete Beams. Structural Control and Health Monitoring, Vol. 32, No. 2, 2025, pp. e3105-e3122.

[4] Asamoto S., Kato K., Maki T., Effect of creep induction at an early age on subsequent prestress loss and structural response of prestressed concrete beam. Construction and Building Materials, Vol. 70, 2014, pp. 158-164.

[5] Purba L.H., Supriyadi B., and Suhendro B., Long-term deflection of prestressed concrete box girder bridges due to creep and shrinkage.

International Journal of GEOMATE, 25(107), 2023, pp. 17-24.
[6] TCVN 3118:1993, Heavy concrete - Method for determining compressive strength. Hanoi: Ministry of Construction, 1993, pp. 1-8.
[7] TCVN 9337:2012, Quality inspection of concrete by ultrasonic method. Hanoi: Ministry of Construction, 2012, pp. 1-12.
[8] Malekzadeh M., Structural Health Monitoring Using Novel Sensing Technologies and Data Analysis Methods. Ph.D. dissertation, University of Central Florida, Orlando, 2014, pp. 1-189.
[9] Phong N.D., Tuyen U.Q., and Osinski P., Risk warning systems for underground mining using IoT solutions: a case study. International Journal of GEOMATE, 27(119), 2024, pp. 100-111.
https://doi.org/10.21660/2024.119.4470
[10] Tokognon C.A., Gao B., Tian G.Y., and Yan Y., Structural health monitoring framework based on Internet of Things: A survey. IEEE Internet of Things Journal, Vol. 4, No. 3, 2017, pp. 619-635.
[11] Abdelgawad A., and Yelamarthi K., Internet of Things (IoT) platform for structure health monitoring. Wireless Communications and Mobile Computing, Vol. 2017, 2017, Article ID 6560797, pp. 1-10.
[12] Iqbal F., Ahmed S., Tariq M.A.B., and Khan M.I., BIM-IoT integration for remote real-time concrete compressive strength monitoring. Ain Shams Engineering Journal, Vol. 15, No. 4, 2024, pp. 102567-102580.
[13] ASTM C1074-19, Standard Practice for Estimating Concrete Strength by the Maturity Method. West Conshohocken: ASTM International, 2011, pp. 1-8.
[14] Tenorio Filho J.R., Gomes R.C., and de Andrade J.J.O., An Automated Wireless System for Monitoring Concrete Structures Based on Embedded Electrical Resistivity Sensors. Sensors, Vol. 23, No. 21, 2023, Article 8775, pp. 1-18.
[15] Razak A.H.A., Zainal N.Z., and Yusof Z.M., Structural Crack Detection System using IoT. Journal of Electrical Engineering, Vol. 18, No. 2, 2022, pp. 45-52.
[16] Kayal A., Mukherjee B., and Sharma S., Application of IoT based Techniques in Concrete - A review. International Journal of Research and Trends in Innovation, Vol. 10, No. 1, 2025, pp. 45-53.
[17] Cruz H., Rocha P., and Sampaio R., Non-Contact Surface Displacement Measurement for Concrete Samples. Proceedings of the International Conference on Experimental Mechanics, Porto, Portugal, 2019, pp. 151-156.
[18] Resensys LLC, Wireless Building Structural Health Monitoring. Application Note AN-2023-04, Salt Lake City: Resensys, 2023, pp. 1-15.
[19] Utepov Y.B., Tulebekova A.S., Kazkeyev A., Zharassov S., Akhazhanov S., and Akishev M., Hardware-software complex of integrated automatic early warning system of sewer overflow, clogging and vandalism. Patent No. 7576, Kazakhstan, 2021, pp. 1-8.
[20] Rawiwan P., and Kongkitkul W., Prediction of Creep Behavior of HDPE Geogrid Using Combined Temperature-Accelerated Stress Relaxation and Creep Testing. International Journal of GEOMATE, 28(128), 2025, pp. 68-75.
https://doi.org/10.21660/2025.128.g14167
[21] Ngudiyono, Suhendro B., Awaludin A., and Triwiyono A., Creep shear deformation of glued-laminated bamboo. International Journal of GEOMATE, 19(73), 2020, pp. 185-192.
https://doi.org/10.21660/2020.73.42823
[22] Baskari T.L., Zakaria Z., Sulaksana N., and Muljana B., Study on rheological constitutive model of Cililin volcanic clay, Indonesia in relation to long-term slope stability. International Journal of GEOMATE, 21(86), 2021, pp. 40-47.
https://doi.org/10.21660/2021.86.j2269
[23] Ngoc T.N., Experimental investigation of creep behaviour of saturated soft clay subjected static loading. International Journal of GEOMATE, 25(108), 2023, pp. 81-88.
https://doi.org/10.21660/2023.108.3894
[24] Chen B., Li Z., Liu C., Du C., and Jiang D., Study on creep characteristics of salt rock under unloading conditions. International Journal of GEOMATE, 19(75), 2020, pp. 215-224.
https://doi.org/10.21660/2020.75.43899
[25] CEB-FIP, Model Code 2010, Lausanne: International Federation for Structural Concrete (fib). 2010, pp. 1-434.
[26] TCVN 3015:1993, Heavy concrete mixtures - Sampling, preparation, and curing of test specimens. Hanoi: Ministry of Construction, 1993, pp. 1-7.
[27] TCVN 4506:2012, Water for concrete and mortar - Technical requirements. Hanoi: Ministry of Construction, 2012, pp. 1-6.
[28] Taffese W.Z., Sistonen E., and Puttonen J., Caustic condition monitoring of concrete structures using fiber optic sensors. Proceedings of the International Conference on Structural Health Monitoring, Stanford, USA, 2019, pp. 234-241.